Glutamatergically Induced Pattern of Ca^{2+} Driving Potential as a Mechanism of Postsynaptic Plasticity

S. M. Korogod and L. P. Savtchenko
International Center of Molecular Physiology, Dniepropetrovsk Division, National Academy of Sciences of Ukraine, 320625 Dniepropetrovsk, Ukraine, and Unite de Neurocybernetique Cellulaire, UPR 9041 CNRS, 13009 Marseille, France

ABSTRACT Simulation studies were performed in a model of neuronal dendrite with Na^+ and K^+ channels and with ionotropic and metabotropic glutamate receptors. The ionotropic receptors were either *N*-methyl-D-aspartate (NMDA)-sensitive, voltage-dependent, and permeable to Ca^{2+}, Na^+, and K^+, or non-NMDA-sensitive, voltage-independent, and permeable to Na^+ and K^+. The metabotropic receptors provided a catalytic effect on Ca^{2+}-induced Ca^{2+} release from intracellular stores. Local intracellular concentration $[Ca^{2+}]_i$ in the cytoplasm was changed because of exchange with the stores, axial diffusion, and transmembrane inward passive and outward pump fluxes. Tonic activation of ionotropic and metabotropic receptors in a particular range of intensities triggered the formation of spatially periodic $[Ca^{2+}]_i$ hot and cold bands arising from an initial uniform state. The period and width of the bands were smaller at higher levels of tonic NMDA activation and higher metabotropically controlled rates of Ca^{2+}-induced Ca^{2+} release. The bandwidths also depended on the dendrite diameter, the specific membrane, and cytoplasm resistivity. This activity-induced pattern led to long-term, spatially inhomogeneous change in local excitatory postsynaptic potentials (EPSPs) of NMDA synapses phasically activated with the same presynaptic intensity. The phasic EPSPs were potentiated if the synapse occurred in the hot band.

INTRODUCTION

Long-lasting activity-dependent changes in synaptic effectiveness play a fundamental role in information storage in the brain (Bliss and Collingridge, 1993; Malenka and Nicoll, 1993). Cellular mechanisms of reversible change in synaptic strength (i.e., synaptic plasticity) remain disputable. Both pre- and postsynaptic sites of these changes are hypothesized (Lynch and Bliss, 1986; Smith, 1987). An essential role in the postsynaptic mechanisms is often attributed to the intracellular concentration of free calcium $[Ca^{2+}]_i$ and to changes in this concentration after glutamatergic synaptic activation. Glutamate is known to bind both ionotropic and metabotropic receptors. The ionotropic receptors are distinguished by their selectivity to α-amino-3-hydroxy-5-methyl-4-isoxazolepropionate (AMPA) and *N*-methyl-D-aspartate (NMDA). The NMDA receptor channels provide a transmitter-gated voltage-dependent entrance for Ca^{2+} at the postsynaptic site. Elevation of $[Ca^{2+}]_i$ by influx through NMDA-operated channels during membrane depolarization triggers a multistage intracellular mechanism, producing a long-term increase in synaptic effectiveness (Bliss and Collingridge, 1993; Malenka and Nicoll, 1993; Nicoll and Malenka, 1995). At initial stages, contribution may come from the glutamate activation of G-protein-coupled metabotropic receptors (Bear and Malenka, 1994), leading to the generation of inositol 1,4,5-triphosphate (IP3), known as a catalyzer of Ca^{2+}-induced Ca^{2+} release from the intracellular stores (Ross et al., 1989; Bezprozvanny et al., 1991; Clapham and Sneyd, 1995). The sequence of events that follow $[Ca^{2+}]_i$ elevation remains unclear (Nicoll and Malenka, 1995).

It is known that $[Ca^{2+}]_i$ exhibits rather complex dynamics, including local sparks and puffs (see Bootman and Berridge, 1995, for a review), oscillations (Fewtrell, 1993; Friel, 1995), and waves (Jafee and Brown, 1994; Clapham and Sneyd, 1995). Less is known about the formation of steady spatial patterns of $[Ca^{2+}]_i$. The possibility of such patterns in simulated neuronal dendrites was demonstrated in the conditions of Ca^{2+}-induced Ca^{2+} release from intracellular stores triggered by $[Ca^{2+}]_i$ elevation due to influx through voltage-operated Ca^{2+} channels (Savtchenko and Korogod, 1994). In this study we focus on that kind of phenomenon, induced via ligand-operated ionotropic and metabotropic calcium pathways, and on its consequences for the synaptic strength estimated by local excitatory postsynaptic potentials (EPSPs). In particular, we test the hypothesis specifying the cascade of events that starts from the elevated tonic activity of glutamatergic synaptic inputs and leads to a spatially patterned increase in synaptic effectiveness at postsynaptic sites. This is manifested in a corresponding increase of postsynaptic response to equally intensive phasic presynaptic inputs. The putative cascade is as follows. Tonic activation of glutamatergic synapses has both ionotropic and metabotropic effects. The ionotropic action causes depolarization of the membrane and an increase in $[Ca^{2+}]_i$ by the Ca^{2+} component of excitatory postsynaptic current through NMDA receptor channels. The metabotropic action ultimately leads to activation of IP3-sensitive channels of intracellular stores, allowing Ca^{2+}-induced Ca^{2+} release from the stores. Moderately elevated

Received for publication 22 November 1996 and in final form 10 June 1997.

Address reprint requests to Dr. S. M. Korogod, CNRS, Unite de Neurocybernetique Cellulaire, 280 Bd Sainte-Marguerite, 13009 Marseille, France. Tel.: 33-04-91-75-0200; Fax: 33-04-91-262038; E-mail: korogod@cptsu2.univ-mrs.fr.

0006-3495/97/09/1655/10 $2.00

$[Ca^{2+}]_i$ triggers both a positive feedback mechanism of self-induced release of Ca^{2+} from the stores (Bezprozvanny et al., 1991) and negative feedback mechanisms of Ca^{2+} removal by transmembrane pump and axial electrodiffusion. We show that concerted action of these positive and negative feedbacks can provide conditions for steady patterns of $[Ca^{2+}]_i$ in the form of spatially periodic concentration profiles arising from an initial uniform state. These long-term bandlike variations in $[Ca^{2+}]_i$ cause corresponding variations in the local equilibrium and driving potentials for the Ca component of glutamatergic postsynaptic current. Unlike in the initial uniform state, the postsynaptic effectiveness of equally intensive phasic presynaptic inputs is unequal, increasing at the sites occurring in the "hot bands" of increased driving potentials.

This article starts with the description of our biophysical model of coupled spatiotemporal dynamics of $[Ca^{2+}]_i$, the membrane potential, and the ionotropic NMDA receptor channels. Then the conditions and mechanisms of diffusion instability in the calcium system are defined by bifurcation analysis, and the computed patterns are illustrated. Finally, the consequences of these long-lasting spatial patterns for local EPSPs are demonstrated.

GLOSSARY

d, l diameter and length of cylinder-shaped cell, respectively (μm)

$V(z, t)$ transmembrane potential in $\beta = RT/F$ ($\beta \approx 25$ mV)

V_{Na}, V_K equilibrium potential for sodium and potassium current, respectively (β)

$[Ca^{2+}]_i$ intracellular calcium concentration (μM)

$[Ca^{2+}]_e$ extracellular calcium concentration (mM)

$[\bar{C}a]$ equilibrium concentration of Ca pump (mM)

$e(z, t)$ density of NMDA channels per unit length ($1/\mu$m)

e_{st} average density of NMDA channels per unit length ($1/\mu$m)

C_m specific membrane capacitance ($\mu F/cm^2$)

R_i resistivity of the cytoplasm (Ohm cm)

$D_V = d/(4R_iC_m)$ coefficient of spatial relaxation of voltage (μm^2/ms)

D_{Ca} diffusivity of calcium (μm^2/ms)

D_e lateral diffusivity of NMDA channels in the membrane (μm^2/ms)

N_e electrophoretic charge of NMDA channels (dimensionless number of elementary charges)

G_{Ca}, G_{Na}, G_K calcium, sodium, and potassium conductivities of the membrane unit area, respectively (mS/cm^2)

I_{Ca}^{pass}, I_{Ca}^{pump} passive and active calcium current density, respectively ($mA/(\beta cm^2)$)

I_{Na} and I_K passive sodium and potassium current density, respectively ($mA/(\beta cm^2)$)

χ effective thickness of the submembrane layer (μm)

MODEL

Composition

The neuronal dendrite was cylinder-shaped, with diameter d and length l. Its membrane contained ionotropic and metabotropic glutamate receptors and pumps, as well as voltage-gated sodium and potassium channels. The receptors, pumps, and channels were distributed uniformly along the dendrite. However, the model also allowed us to take into account the lateral electrodiffusion of NMDA-receptive channels. Intracellular calcium stores were uniformly distributed along the cell. Coupled dynamics of the transmembrane potential, $[Ca^{2+}]_i$, and NMDA channels was described by three one-dimensional reaction-diffusion equations taking advantage of cylindrical symmetry of the cellular processes (Kurata et al., 1989).

Transmembrane potential dynamics

The first equation describes the dynamics of the transmembrane potential:

$$\frac{\partial V}{\partial t} = \frac{d}{4R_iC_m}\frac{\partial^2 V}{\partial z^2} + Q_V \qquad (1a)$$

where $Q_V = -(I_{tot} - I_{Ca}^{pump})/C_m$ is the source function of V. All components of passive transmembrane current I_{tot} were conducted along the electrochemical gradients through voltage- and ligand-operated channels. Voltage-operated Na^+ and K^+ channels were represented by corresponding membrane conductances per unit area, $G_{m,Na}$ and $G_{m,K}$. Because we considered only small deviations of transmembrane voltage from the resting value, these conductances kept their resting values, and the corresponding passive currents were linearized functions of the voltage. Ligand-operated conductances were those of the postsynaptic channels of the glutamatergic synapses. These channels belong to one of the two subpopulations associated with AMPA and NMDA ionotropic receptors. Postsynaptic ionotropic activation of distributed glutamatergic synaptic inputs was defined by the intensity parameter $q(z, t) = p(z, t)\, e(z, t)/e_{st}$, where $p(z, t)$ and $e(z, t)$ were, respectively, the presynaptic activation intensity and the longitudinal density of ionotropic receptors as functions of longitudinal coordinate z and time t, and e_{st} was the average longitudinal density of the receptors. If the receptors were immobile, $e(z, t) = e_{st} = \text{const}$ and $q(z, t) = p(z, t)$. In particular cases, $p(z, t) = 0$ (silent synaptic inputs), $p(z, t) = p \neq 0$ (spatially uniform tonic activation), and $p(z, t) = p(t)\delta(z - z')$, where $p(t) = (\alpha t/\pi)\exp(-\alpha t)$ was the α-function defining time course of intensity changes, and $\delta(z - z')$ was the delta function of Dirac (phasic activation at a site $z = z'$). The AMPA ionotropic receptors were associated with composite Na-K conductance, $G_{ampa} = G_{ampa,Na} + G_{ampa,K}$ (MacDermott and Dale, 1987; Asher and Nowak, 1988a; Collingridge and Lester, 1989). The NMDA ionotropic receptors were associated with composite Ca-Na-K conductance, $G_{nmda} = G_{nmda,Ca} +$

$G_{nmda,Na} + G_{nmda,K}$ (Mayer and Westbrook, 1987; Asher and Nowak, 1988b). The total current through these conductances was thus defined by

$$I_{tot} = G_{Ca}(V - V_{Ca}) + G_{Na}(V - V_{Na}) + G_K(V - V_K)$$

where

$$G_{Ca} = q(z, t)G_{nmda,Ca}$$

$$G_{Na} = F_{m,Na} + q(z, t)(G_{ampa,Na} + G_{nmda,Na})$$

$$G_K = G_{m,K} + q(z, t)(G_{ampa,K} + G_{nmda,K})$$

This was valid in the case of equal AMPA and NMDA subpopulations of glutamate ionotropic receptors. Otherwise, the activation intensity parameter would be different for AMPA and NMDA receptors. Permeability of NMDA-gated channels was 10 times greater for Ca^{2+} than for Na^+ and K^+. It changed in a voltage-dependent manner because of removal of Mg^{2+} block by the membrane depolarization. We assumed $G_{nmda,Ca}(V) = \bar{G}_{Ca}/(1 + [Mg^{2+}]\exp(2 - V)/3)]$, where the fixed extracellular magnesium concentration was $[Mg^{2+}] = 2$ mM (Holmes and Levy, 1990). In this model, the equilibrium potential of calcium transmembrane current changed because of variable $[Ca^{2+}]_i$, $V_{Ca} = 0.5 \ln([Ca^{2+}]_e/[Ca^{2+}]_i)$.

The electrogenic Ca pump generated the only active current against electrochemical gradient: $I_{Ca}^{pump} = F\chi([\bar{Ca}] - [Ca^{2+}]_i)/(\beta t_{pump}(V))$, where $t_{pump}(V) = 20 \exp(5V/7)$ was the voltage-dependent time constant (Yamada et al., 1989).

Intracellular Ca^{2+} dynamics

The dynamics of $[Ca^{2+}]_i$ in a thin submembrane layer was described by the diffusion equation

$$\frac{\partial[Ca^{2+}]_i}{\partial t} = D_{Ca}\frac{\partial^2[Ca^{2+}]_i}{\partial z^2} + Q_{Ca} \qquad (1b)$$

In Eq. 1b the source function $Q_{Ca} = -(J_{Ca}^{pass} - J_{Ca}^{pump}) + W$ defined contributions to change in $[Ca^{2+}]_i$ from three local radial fluxes per unit length of the dendrite:

1) $J_{Ca}^{pass} = \beta I_{Ca}^{pass}/F\chi$ came from the passive current through NMDA channels $I_{Ca}^{pass} = q(z, t)G_{nmda,Ca}(V - V_{Ca})$;
2) $J_{Ca}^{pump} = ([\bar{Ca}] - [Ca^{2+}]_i)/t_{pump}(V)$ was the pump efflux; and
3) $W = \gamma[Ca^{2+}]_i(0.2 - [Ca^{2+}]_i)([Ca^{2+}]_i - 1.4)$ came from the flux from intracellular stores through IP3-sensitive Ca^{2+}-dependent channels.

In 3) γ was the rate constant of depletion modulated by metabotropic activation of the stores. This flux corresponded to uniformly distributed stores with bell-shaped $[Ca^{2+}]_i$ dependence of the opening probability of the store channels in the operative range of concentrations (Bezprozvanny et al., 1991). In the absence of metabotropic action, the depletion rate constant took its "resting" value of $\gamma =$ 6.0. Activation of metabotropic receptors was simulated as an increase in γ above this resting value.

Dynamics of mobile channels

To take into account the lateral redistribution of NMDA channels as protein molecules bearing intracellularly exposed electrophoretic charge N_e, one can assume variable longitudinal density of NMDA receptors $e(z, t)$. Changes in $e(z, t)$ due to the lateral electrodiffusion of NMDA channels were described by the following equation (Fromherz and Zimmermann, 1995):

$$\frac{\partial e}{\partial t} = D_e\frac{\partial^2 e}{\partial z^2} + N_e\frac{\partial}{\partial z}\left(e\frac{\partial V}{\partial z}\right) \qquad (1c)$$

In this model, changes in Na^+ and K^+ membrane conductances due to changes in NMDA channel density $e(z, t)$ were neglected, as Na^+ and K^+ permeabilities of NMDA channels were one order lower than Ca^{2+}.

Initial and boundary conditions

Equations 1 were defined in the finite domain $[0, l]$ with zero flux boundary conditions. The initial longitudinal distributions of $[Ca^{2+}]_i$ and V were uniform random.

Method of numerical solution and parameters of the model

The Crank-Nicholson method was used for numerical solution of Eqs. 1a,b as described by Smith (1985).

List of fixed model parameters

$d = 0.4$ μm, $l = 200$ μm, $\chi = 0.05$ μm
$C_m = 1$ μF/cm^2, $R_i = 200$ Ohm cm
$V_{Na} = 2.3$ β, $V_K = -5.9$ β
$G_{m,Na} = 1.5$ mS/cm^2, $G_{m,K} = 2$ mS/cm^2
$G_{ampa,Na} + G_{nmda,Na} = 0.1$ mS/cm^2, $G_{ampa,K} + G_{nmda,K} = 0.1$ mS/cm^2
$\bar{G}_{Ca} = 1$ mS/cm^2
$D_V = 5000$ μm^2/ms, $D_{Ca} = 1$ μm^2/ms
$[Ca^{2+}]_e = 1.2$ mM, $[\bar{Ca}] = 0.2$ μM, $\alpha = 1$

The values of variable parameters $q(z, t)$ and γ are specified below in each case.

CONDITIONS OF DIFFUSION-DRIVEN INSTABILITY

Immobile channels

System 1 exhibited the diffusion-driven instability if the homogeneous steady state (V_{st}, $[Ca]_{st}$) was stable in relation to spatially homogeneous perturbations, but unstable to an inhomogeneous perturbation (Turing, 1952; Murray, 1989). The nontrivial steady state (V_{st}, $[Ca]_{st}$) was defined from Eq.

1a,b by setting $\partial V/\partial t = 0$, $\partial[Ca^{2+}]_i/\partial t = 0$, $\partial^2 V/\partial z^2 = 0$, $\partial^2[Ca^{2+}]_i/\partial z^2 = 0$. The linear analysis of stability of this uniform steady state in relation to small spatial perturbations gave the following. For smooth initial data, the solution of the linearized problem was the sum of functions $\exp(\lambda t)\cos(N\pi z/l)$, where $\lambda = \lambda(N)$ was the rate constant of growth of the Fourier component of initial perturbation with the wave number N and the spatial mode $k = N\pi/l$. To analyze the growth of these Fourier components (Murray, 1989), we looked for solutions to the linearized system (1) in the form

$$\text{Const}\begin{pmatrix} V - V_{st} \\ [Ca^{2+}]_i - [Ca]_{st} \end{pmatrix}\exp(\lambda t)\cos(N\pi z/l)$$

The dispersion relation was

$$\begin{bmatrix} m_{11} - \lambda - D_V k^2 & m_{12} \\ m_{21} & m_{22} - \lambda - D_{Ca}k^2 \end{bmatrix} = 0 \qquad (2)$$

where the linearization coefficients were

$$m_{11} = \frac{\partial Q_V}{\partial V} = -\frac{1}{C_m}\left(G_K + G_{Na} + \frac{\partial(I_{Ca}^{pass} - I_{Ca}^{pump})}{\partial V}\right),$$

$$m_{12} = \frac{\partial Q_V}{\partial [Ca^{2+}]_i} = -\frac{1}{C_m}\frac{\partial(I_{Ca}^{pass} - I_{Ca}^{pump})}{\partial [Ca^{2+}]_i}$$

$$m_{21} = \frac{\partial Q_{Ca}}{\partial V} = -\frac{\partial(J_{Ca}^{pass} - J_{Ca}^{pump})}{\partial V},$$

$$m_{22} = \frac{\partial Q_{Ca}}{\partial [Ca^{2+}]_i} = -\frac{\partial(J_{Ca}^{pass} - J_{Ca}^{pump})}{\partial [Ca^{2+}]_i} + \frac{\partial W}{\partial [Ca^{2+}]_i}$$

Linear stability of the point system with $D_V = D_{Ca} = 0$ was guaranteed if $m_{11} + m_{22} < 0$ and $m_{11}m_{22} - m_{12}m_{21} > 0$ (Turing, 1952; Murray, 1989). The steady state (V_{st}, $[Ca]_{st}$) was unstable in relation to spatially nonuniform perturbations, if there existed at least one wave number N such that $\mathrm{Re}(\lambda(k^2)) > 0$. This meant that the linearized system promoted growth of the mode with wave number N from the whole Fourier spatial spectrum of the initial perturbation. The uniform steady state lost stability, if the free term of dispersion relation was negative,

$$F(k^2) = D_V D_{Ca}k^4 - k^2(D_V m_{22} + D_{Ca}m_{11}) + m_{11}m_{22} - m_{12}m_{21} < 0 \qquad (3)$$

for some k.

Because we required stability of the point model, the only possibility for $F(k^2)$ to be negative was

$$D_V m_{22} + D_{Ca}m_{11} > 0 \qquad (4)$$

The inequality in Eq. 4 and $m_{11} + m_{22} < 0$ implied opposite signs for m_{11} and m_{22}. Because in our model $m_{11} < 0$ always held (the contrary would be true only for the excitable membrane capable of regenerative discharge), Eq. 4 was true when $m_{22} > 0$. The inequality $m_{22} > 0$ was true in the case when $\partial Q_{Ca}/\partial[Ca^{2+}]_i > 0$, that in turn was possible when $\partial W/\partial[Ca^{2+}]_i > 0$ and/or $\partial(J_{Ca}^{pass} - J_{Ca}^{pump})/\partial[Ca^{2+}]_i < 0$. Because

$$\frac{\partial(J_{Ca}^{pass} - J_{Ca}^{pump})}{\partial [Ca^{2+}]_i} = \frac{1}{t_{pump}(V)} + \frac{\beta q G_{nmda,Ca}}{2F\chi[Ca]_{st}}$$

was essentially positive, the inequality $m_{22} > 0$ held when $\partial W/\partial[Ca^{2+}]_i > 0$, which took place when Ca^{2+}-induced Ca^{2+} release was triggered. The inequality in Eq. 3 defined the range of (k_1^2, k_2^2) of the spatial modes that could grow, i.e., a finite band of unstable modes $\cos(\pi Nz/l)$ for finite N. The fastest growing mode N corresponded to $k = N\pi/l$ the nearest to k_m, the minimum point of the $F(k^2)$ curve. In our case, $F \to F_{min}$ when $k^2 \to k_m^2$, where $k_m = 0.5(m_{22}/D_{Ca} + m_{11}/D_V)$ was the spatial mode of the fastest growing mode with the wave number

$$N = \frac{l}{\pi\sqrt{2}}\sqrt{\frac{m_{11}}{D_V} + \frac{m_{22}}{D_{Ca}}}$$

If the total membrane conductance ($-C_m m_{11}$) and therefore the absolute value of negative m_{11} increased, then N decreased. Conversely, if positive m_{22} increased, then N also increased. The number of periods N (bands) depended on D_V, defined particularly by the cytoplasm resistivity R_i and the dendritic diameter d.

Mobile channels

The dispersion relation for the extended system of equations (Eq. 1a,b,c) in the neighborhood of the steady state (V_{st}, $[Ca]_{st}$, e_{st}) was

$$\begin{bmatrix} m_{11} - \lambda - D_V k^2 & m_{12} & m_{13} \\ m_{21} & m_{22} - \lambda - D_{Ca}k^2 & m_{23} \\ -D_e N_e e_{st} k^2 & 0 & -\lambda - D_e k^2 \end{bmatrix} = 0$$

where the modified linearization coefficients are

$$m_{13} = -I_{Ca}^{pass}/(C_m e_{st}), \quad m_{23} = -(\beta I_{Ca}^{pass})/(F\chi e_{st})$$

For this modified model,

$$N = \frac{l}{\pi\sqrt{2}}\sqrt{\frac{m_{11} + N_e I_{Ca}^{pass}/C_m}{D_V} + \frac{m_{22}}{D_{Ca}}} \qquad (5)$$

As follows from Eq. 5, the patterns that occurred when the channels were mobile differed from those that occurred when channels were immobile. This difference was due to the contribution of the term $N_e I_{Ca}^{pass}/C_m$, which brought dependence of the spatial period on the electrophoretic charge N_e and the average density of NMDA channels (see Model). The formation time of the spatial pattern was very short as compared to the known time of channel installation into or release from the plasma membrane. Because of that average density of NMDA channels, e_{st} remained unchanged during the time of the pattern formation.

RESULTS

Pattern formation

In our model pattern formation was governed by the driving term, which was the value of the derivative $\partial W/\partial[Ca^{2+}]_i$ taken at the steady-state point (V_{st}, $[Ca]_{st}$). This derivative has the meaning of sensitivity of Ca^{2+}-induced Ca^{2+} release to a change in $[Ca^{2+}]_i$. If this term did not obey the condition of diffusion-driven instability $\partial W/\partial[Ca^{2+}]_i > 0$, the pattern could not be formed by variation of any other terms. Specific values of the driving term (see below) depended explicitly on γ (as W was an explicit function of γ as the parameter) and implicitly on both γ and q (as the coordinates of the steady-state V_{st}, $[Ca]_{st}$ depended on γ and q). We have scanned the plane of the free parameters (γ, q) by fixing γ and varying q and found the region on the border of which the driving term took its critical values as defined from Eq. 4. This is shown in Fig. 1. The pattern occurred if (γ, q) were inside the tracing intervals, where inequality Eq. 4 is valid. With (γ, q) outside this domain, the system was stable in relation to spatially uniform perturbations (the local stability), because the value $[Ca^{2+}]_i = 0.6$ μM was reached, making pattern formation impossible.

Reference steady state

In the reference steady state, there was no postsynaptic activation of either iono- or metabotropic receptors, assuming $q(z, t) = 0$ and the "resting" depletion rate $\gamma = 6$. The longitudinal distributions of $[Ca^{2+}]_i$, transmembrane potential and membrane conductances were uniform. The corresponding null clines are shown in Fig. 2 *a*. The intersection of the null clines $Q_{Ca} = 0$ and $Q_V = 0$ defined the coordinates of the local steady state ($V_{st} = -2.4$ and $[Ca]_{st} = 0.2$ μM). Here V_{st} is the resting potential defined by equilibrium between passive currents through $G_{m,Na}$ and $G_{m,K}$ conductances, and $[Ca]_{st}$ is the equilibrium concentration defined by zero calcium exchanges across the membrane and with the stores. The linearization coefficients were $m_{11} = -3.5$, $m_{12} = -1.0356$, $m_{21} = 0$, and $m_{22} = -3.5547$. The negative m_{22} indicated that $[Ca]_{st}$ was too low to induce the critical rate of calcium release from the stores and therefore that the pattern formation was impossible. The driving term, $\partial W/\partial[Ca^{2+}]_i$, in that case was 1.44.

Triggering via ionotropic receptors

In the absence of metabotropic action ("resting" value of $\gamma = 6.0$), uniform tonic ionotropic activation $q(z, t) = q$ led to a uniform increase in synaptic conductance $G_s = q(G_{ampa} + G_{nmda})$. With $q = 3.0$ there was a critical elevation of $[Ca^{2+}]_i$ by influx through NMDA channels, and the critical rate of the Ca^{2+}-induced Ca^{2+} release was reached, exceeding the rate of $[Ca^{2+}]_i$ decrease by the pump extrusion and the axial diffusion. This triggered the pattern formation. The corresponding null clines are shown in Fig.

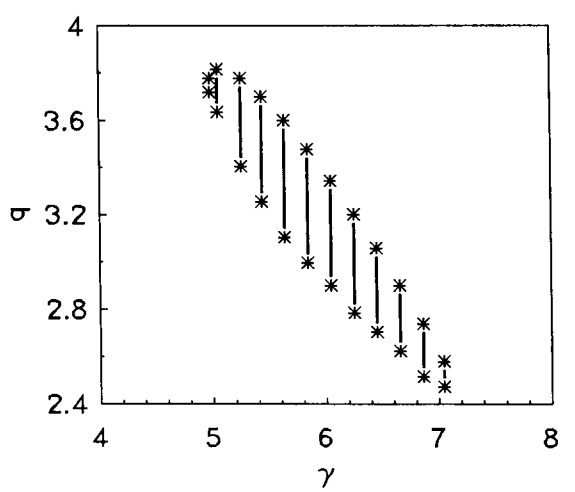

FIGURE 1 The domain of the intensity parameters of tonic glutamatergic ionotropic and metabotropic activation (q, γ) defining the driving term $\partial W/\partial[Ca^{2+}]_i$ that is sufficient for the pattern formation. The domain was traced at different fixed values of the metabotropically modulated rate constant of the Ca stores depletion γ (*abscissa*) by change in the ionotropic activation intensity q (*ordinate*) to see where the inequality in Eq. 4 was true. The critical value of the driving term was at the ends of the intervals (marked by *asterisks*), where the left-hand side of Eq. 4 was equal to 0. The pattern did not occur for any q if $\gamma < 4.9$ or $\gamma > 7.2$.

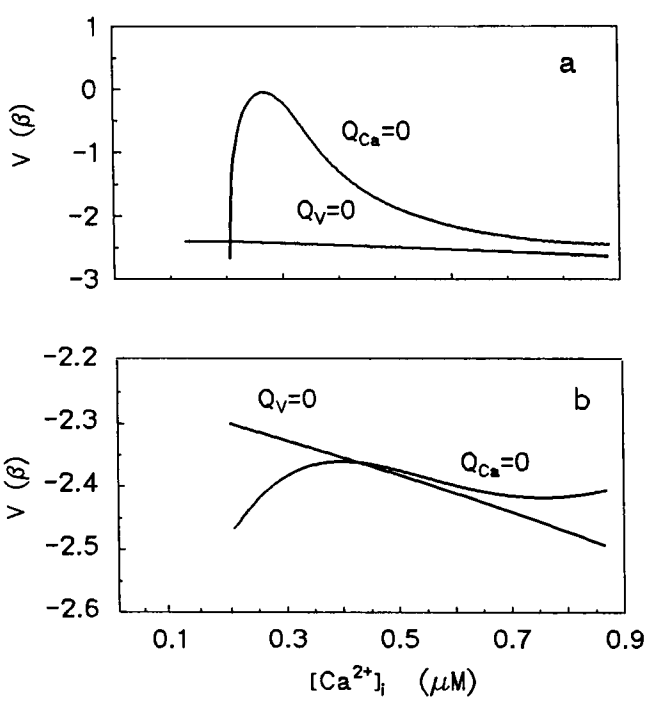

FIGURE 2 Null clines $Q_V = 0$ and $Q_{Ca} = 0$ of the phase portrait of the point model ($D_V = D_{Ca} = 0$) corresponding to the reference uniform steady state maintained in the absence of glutamatergic activation (*a*) and to the pattern formation triggered solely by tonic ionotropic activation at the supercritical level $q = 3$ (*b*). The depletion rate of calcium stores kept its resting value of $\gamma = 6$ in both cases, as metabotropic activation was absent. (*Abscissa*) Intracellular Ca^{2+} concentration in μM. (*Ordinates*) The transmembrane potential in β.

2 b, where new coordinates of the steady state were $V_{st} = -2.352\beta$, $[Ca]_{st} = 0.428$ μM, and the driving term, $\partial W/\partial[Ca^{2+}]_i$, was 3.24. In this steady state, the linearization coefficients were $m_{11} = -3.7364$, $m_{12} = -1.0315$, $m_{21} = 1.0011$, $m_{22} = 0.0285$. Unlike in the previous case, m_{22} was positive, indicating a supercritical rate of Ca^{2+} release from the stores. Thus the spatial pattern occurred from the initial white noise in the form of spatially periodic steady distribution of $[Ca^{2+}]_i$, V, and the driving potential $(V - V_{Ca})$ (Fig. 3, *solid line*). Other examples with a greater, supercritical tonic synaptic activation ($q = 3.1$) are illustrated in Fig. 3 (*dotted line*). In this case, the coordinates of the steady state were $V_{st} = -2.358$ β and $[Ca]_{st} = 0.43$ μM. The driving term, $\partial W/\partial[Ca^{2+}]_i$, was 3.25. In the pattern, the dominating mode was that with the wave number $N = 8$. This was in agreement with the fastest growing mode predicted by the linear analysis, defining $N = 8$ as the point where the free term (Eq. 3) had its minimum $F(N) = -0.56$ ms^{-2}.

Triggering via metabotropic pathway

Increasing γ made it possible to trigger the formation of a spatially nonuniform pattern at a lower level of synaptic activation. At the same critical level of $q = 3.0$, as illustrated by Fig. 3 (*solid line*), the greater value of $\gamma = 6.1$ led to decrease in the spatial period of the hot and cold bands. The steady-state coordinates were $V_{st} = -2.361\beta$ and $[Ca]_{st} = 0.432$ μM. The driving term, $\partial W/\partial[Ca^{2+}]_i$, in this case was 3.30. The mode $N = 10$ of a shorter spatial period was dominating (Fig. 4, *solid line*). This mode was also in agreement with that predicted by linear analysis (not illustrated). With $\gamma = 6.1$ and higher ionotropic activation $q = 3.1$, corresponding to Fig. 3 (*dotted line*), the model produced the pattern shown in Fig. 4 (*dotted line*). The steady-state voltage and concentration were $V_{st} = -2.362\beta$ and $[Ca]_{st} = 0.433$ μM, and the driving term was $\partial W/\partial[Ca^{2+}]_i = 3.31$. In agreement with linear analysis prediction, the mode with $N = 11$ dominated.

Contribution from mobile channels

According to Eq. 5, lateral electrodiffusion of the channels could change the pattern, but these changes occurred in a time scale on the order of 1 h. This was much longer than the time scale of pattern formation defined by electrical relaxation (10^{-2} s) and ion electrodiffusion (10 s) in the neuron. Thus the pattern formed by the two faster mechanisms was further transformed by the slow redistribution (condensation in the "hot bands") of the mobile channels due to their lateral electrodiffusion.

Consequences for phasic synaptic inputs

Local EPSPs were computed in response to phasic glutamatergic activation of ionotropic receptors at two different

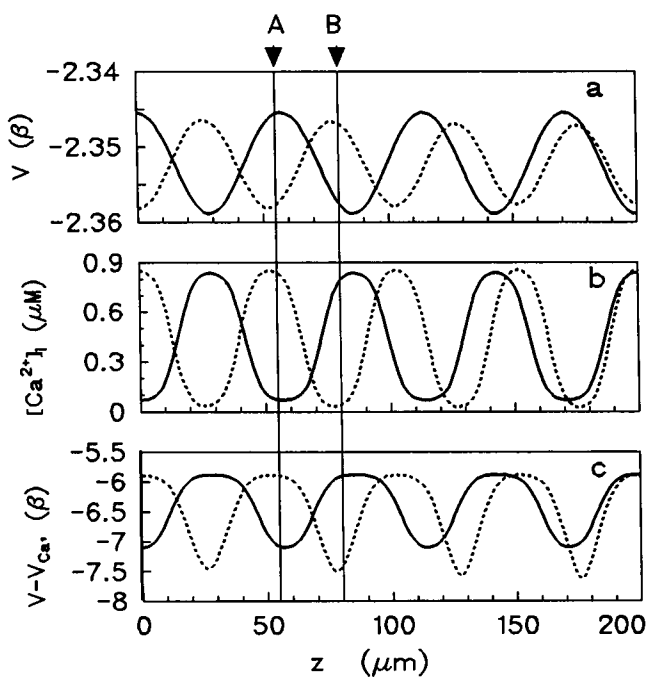

FIGURE 3 Spatial patterns of the transmembrane potential (a), the intracellular Ca^{2+} concentration (b), and the driving potential of Ca^{2+} current (c) as function of the axial coordinate z (*abscissa*, μm) along the cell, occurring at two levels of tonic ionotropic activation of NMDA conductances, $q = 3$ (*solid lines*) and $q = 3.1$ (*dotted lines*) performed without metabotropic activation. Arrows A and B indicate the two synaptic sites phasically activated in other experiments (Fig. 5).

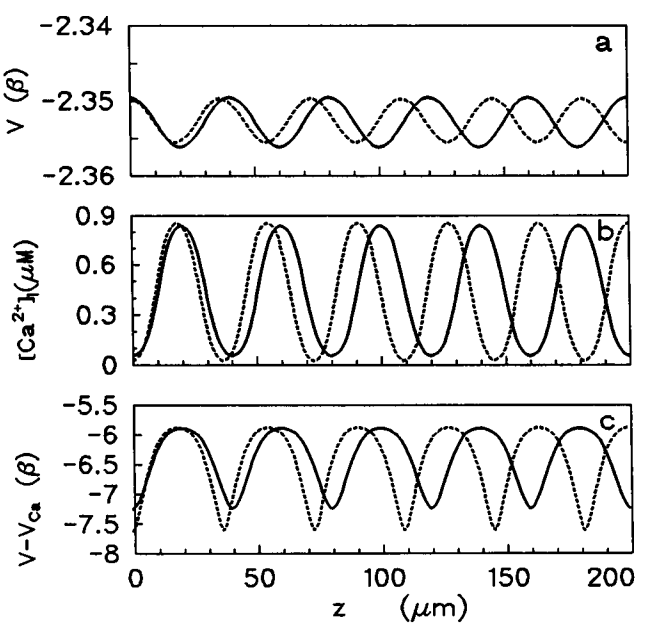

FIGURE 4 Spatial patterns of the transmembrane potential (a), the intracellular Ca^{2+} concentration (b), and the driving potential of Ca^{2+} current (c) as function of the axial coordinate z (*abscissa*, μm) along the cell, occurring at two levels of tonic ionotropic activation of NMDA conductances, $q = 3$ (*solid lines*) and $q = 3.1$ (*dotted lines*) performed with an increased depletion rate of the calcium stores ($\gamma = 6.1$) due to metabotropic activation.

synaptic sites A and B situated in $z' = 55$ and 80 μm from the left end, respectively (Fig. 5). The phasic activation was performed at three different levels of tonic activity (the ionotropic intensity parameter $q = 0$, 2.9 and 3.1). Other conditions were the same as those described above in the first section, above (see also Fig. 3). In homogeneous steady states (subcritical $q = 0$ and 2.9), the two synapses were at the same condition of equal driving potential. When the pattern formed (supercritical $q = 3.1$; Fig. 3, *dotted line*) the conditions at those synaptic sites became different, so that synapse A was in the cold band and synapse B was in the hot band. The largest changes in the local EPSP took place at the site of hot-band synapse B. When this synapse was activated at a resting potential of −60 mV (no tonic activation, $q = 0$), the local EPSP reached −55.7 mV (giving 4.3 mV amplitude of phasic depolarization). The subcritical tonic activation ($q = 2.9$) brought the membrane potential to the new uniform steady level of −58.6 mV. In this case the local phasic EPSP of synapse B reached −54.4 mV (the amplitude of 4.2 mV as counted from that steady level). A small increase in the tonic activity (up to $q = 3.1$) led to the pattern formation with the steady membrane potential −58.4 mV at the site of hot-band synapse B, where the EPSP reached −53 mV (amplitude 5.4 mV). Thus, in the hot band, with a very small 0.2-mV shift in the steady membrane potential, the potentiation of phasic EPSP reached 1.2 mV, that is, 28.6% of the amplitude in the subcritical homogeneous state.

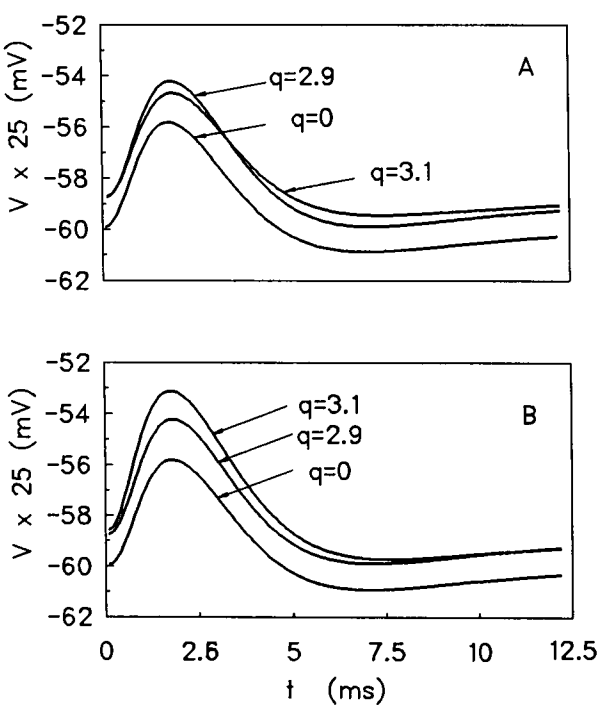

FIGURE 5 EPSPs evoked at the synaptic site phasically activated with the same intensity at three different levels of tonic spatially uniform ionotropic activation ($q = 0$, $q = 2.9$, $q = 3.1$), which is performed without metabotropic activation. *A* and *B* correspond to the synaptic sites indicated in Fig. 3. The cell membrane was in the steady state of the reference uniform polarization ($q = 0$), the uniform depolarization ($q = 2.9$), or the spatially periodic pattern ($q = 3.1$), which was shown by the dotted line in Fig. 3, with synapses *A* and *B* in the cold and hot bands, respectively, of the driving potential.

At the site of synapse A, tonic and phasic membrane potentials were practically the same as those at the site B for subcritical $q = 0$ and 2.9. For the supercritical $q = 3.1$, when site A occurred in the cold band, the steady membrane potential here practically did not shift from its former subcritical level of −58.6 mV ($q = 2.9$), but the amplitude of phasic EPSP was slightly reduced (0.4 mV or 9% depression). Thus the outcome of the pattern formation induced by tonic activation of NMDA receptors was the potentiation of local phasic EPSPs in the hot band that was 3 times greater than the depression of those in the cold bands.

In these experiments, the difference between hot- and cold-band EPSP was studied at two spatially separated sites A and B, where the input conductances of the dendrite were slightly different. To avoid the contribution of this difference and to see the consequences for the same postsynaptic site to occur in either the hot or cold band, the same phasic activation of synapse A was performed for the two different patterns shown in Fig. 3. Depending on the spatial period of the pattern, synapse A occurred in either the hot or cold band of the calcium driving potential (Fig. 3, *solid* or *dotted line*, respectively). The same relationships between hot-band and cold-band EPSPs with dominating potentiation were observed (not illustrated).

DISCUSSION

Postsynaptic efficacy factors

Synaptic strength could be changed both pre- and postsynaptically. We focus on postsynaptic changes of local EPSPs, which depend on several factors: 1) the subsynaptic conductance of transmitter-activated channels, 2) the driving potential of the postsynaptic current, and 3) the input conductance of the cell at the synaptic site (with the contribution of extrasynaptic conductances). Pure ionotropic action of neurotransmitter directly increases the subsynaptic and the input conductances and indirectly (because of a voltage drop by synaptic current) decreases the driving potential. Such an ionotropic effect, in combination with metabotropic activation of Ca-induced Ca release from intracellular stores in our model, caused the formation of a bandlike steady pattern of calcium concentration and driving potential. The efficacy of phasic synaptic input was potentiated in the hot bands of increased driving potential (decreased $[Ca^{2+}]_i$). The pattern was induced by tonic steady and homogeneous synaptic input to the uniform dendrite because of diffusion-driven instability in the system of control of intracellular Ca^{2+}, including exchange with the stores, and passive and pump Ca currents across the plasma membrane.

Mechanism of pattern formation

The mechanism of the pattern formation can be explained by analogy with reaction-diffusion systems (see Murray,

1989, for a review). In two-component reaction-diffusion systems with the inhibitor and the activator, a pattern occurs if during the same time the inhibitor diffuses (spreads) farther away than the activator. The reaction is thus potentiated in the "hot" region where the slow activator dominates and is depressed at some distance in the "cold" region where the fast inhibitor dominates. The size and shape of the hot and cold regions depend on the relation between diffusivities of the activator and inhibitor, rate constants of the reaction, boundary conditions, etc. (Murray, 1989). The fast (long distance) and slow (short distance) spreading components are the transmembrane potential ($D_V = 5000\ \mu m^2/ms$) and intracellular Ca^{2+} ($D_{Ca} = 1\ \mu m^2/ms$), respectively. For the pattern formation, $[Ca^{2+}]_i$ should work as the activator, and the potential as the inhibitor. The potential always plays the role of the inhibitor. A local increase in $[Ca^{2+}]_i$ decreases the depolarizing equilibrium potential V_{Ca} and thus produces a hyperpolarization of the membrane. The hyperpolarization decreases NMDA conductance with a dominating Ca component. The events are reversed when $[Ca^{2+}]_i$ is decreased. Therefore the transmembrane potential provides negative feedback, preventing $[Ca^{2+}]_i$ from changing. Unlike the potential, $[Ca^{2+}]_i$ could serve as either the inhibitor or the activator. The actual role is manifested by the sign of $m_{22} = \partial Q_{Ca}/\partial[Ca^{2+}]_i$ in the vicinity of the steady state, that is Ca sensitivity of the total Ca flux to the submembrane layer of the cytoplasm. Negative or positive m_{22} means a decrease or increase in the flux with an increase in $[Ca^{2+}]_i$, which corresponds to autoinhibition or autocatalysis, respectively. If both voltage and $[Ca^{2+}]_i$ act as inhibitors, the system relaxes to the homogeneous steady state after inhomogeneous perturbation. If the voltage remains as the inhibitor and $[Ca^{2+}]_i$ becomes the activator, then the pattern occurs. As one can see from the composition of Q_{Ca}, the sign of m_{22} becomes positive only when the driving term $\partial W/\partial[Ca^{2+}]_i$ becomes positive and greater than the module of the term $\partial(J_{Ca}^{pump} - J_{Ca}^{pass})/\partial[Ca^{2+}]_i$, which is always negative. In these conditions, a fluctuation increase $\delta[Ca^{2+}]_i$ induces changes in the local calcium fluxes. The two fluxes removing Ca^{2+} are increased. They are the diffusion flux $kD_{Ca}\delta[Ca^{2+}]_i$ (where $k = N\pi/l$) and the pump efflux J_{Ca}^{pump}. Of the other two fluxes bringing Ca^{2+}, the passive NMDA influx J_{Ca}^{pass} is decreased and the flux of Ca-induced Ca release from the stores χW is increased. The latter provides a dominating increase of the fluctuation, so that the pattern with spatial length $1/k$ occurs. The critical value of the driving term, 3.24, corresponded to the molar flux from the stores, $\chi W = 4.5 \times 10^{-7}\ mol/(m^2 s)$.

Model assumptions and their influence on pattern formation

For pattern formation with the described mechanism, the assumed shape of the kinetic function W of Ca exchange with intracellular stores is important. This function has a negative bell-shaped section in the range of $[Ca^{2+}]_i$ from 0 to 200 nM, a positive bell-shaped section in the range from 200 to 1400 nM, a monotonically decaying negative section in the range of $[Ca^{2+}]_i$ exceeding 1400 nM. Negative and positive values of W mean calcium uptake and release by the stores. The positive bell-shaped section of W corresponds to Ca^{2+}-induced Ca^{2+} release, which is critically important for the described mechanism of the pattern formation. This section directly corresponds to the known calcium response curves of IP3 receptor channels of the intracellular stores (Bezprozvanny et al., 1991), as found in the Purkinje cells of the cerebellum (Ross et al., 1989). Negative W corresponds to Ca^{2+} uptake by the stores (replenishment) when the concentration falls below a certain level (Jafee and Brown, 1994).

Another assumption of the model was linearization of nonlinear Na and K conductances of the dendritic membrane. This simplification was justified by small deviations of transmembrane voltage from the resting value, so that these conductances did not change their resting values too much. As follows from the results shown in Figs. 3 and 5, the steady shifts in the transmembrane potential from the original resting value during tonic activation did not exceed 1.25 mV. Even for the high density of these channels needed for generation of the action potentials, this shift would lead to only a 2% change in the conductance. We did not simulate spike propagation in the dendrites; therefore the channel density is relatively low and the assumption is valid. We did not include voltage-gated calcium conductance for the same reasons as for the model of long-term potentiation associated with NMDA receptor-mediated Ca^{2+} influx and $[Ca^{2+}]_i$ changes (Holmes and Levy, 1990).

Different time scales of long-term changes in synaptic strength

In fact, three different time scales of changes in the synaptic strength are defined by kinetics of the three main state variables of the model during pattern formation. The transmembrane voltage relaxation has the fastest kinetics, occurring in a time scale on the order of several milliseconds. The moderate kinetics with a time scale of several seconds is typical for the ion diffusion. The redistribution of the mobile channels due to lateral electrodiffusion in the membrane, if it exists, has the slowest kinetics, which defines changes in the synaptic strength lasting for hours. In our model, the pattern formation is mainly defined by the kinetics of ion redistribution in the intracellular space. If tonic activity is interrupted, the pattern induced by this activity will relax over a time period approximately equal to that during which it was formed. The corresponding changes in synaptic efficacy will exist during this entire time (several tens of seconds). If the channels are mobile, they can be redistributed over a longer time scale, and the pattern will relax over a period of hours after the end of the tonic activation. These short, long, and very long-term reversible changes in the synaptic strength can provide flexible possibilities for activity-dependent information storage in the brain.

Physiological feasibility of the proposed mechanism of long-term plastic changes in synaptic strength

The effects described in this paper were demonstrated in a simulated long, thin dendrite. They are likely to occur in thin peripheral branches of complex dendritic arborizations. These branches are often out of the scope of electrophysiological and optical recordings. The described mechanism of activity-dependent change in the synaptic strength may be an important mechanism of the local signal processing in the distal dendrites (Shepherd, 1972), although direct consequences for the somatic generator zone might be small. In principle, there are no obstacles to the occurrence of similar phenomena in thick dendrites. Our choice of thin branches was justified by the intention to demonstrate the possible mechanism of nonuniform spatial pattern formation in a geometrically and biophysically uniform system. It is an important emphasis of this work that a nonuniform pattern has dynamic nature and it is not induced by preexisting inhomogeneities in the cell morphology or in the location of intracellular organelles. For the sake of simplicity, we used the cylinder-shaped cell with $d \ll l$ to decrease the dimension of the equations. Using the cell geometry with a greater diameter would lead to the restoration of transactional/circumferential dependence of the pattern (Kurata et al., 1989). As in other reaction-diffusion systems, in the thicker cell the patchlike pattern would be observed, instead of a bandlike pattern. Therefore, the pattern will be formed by "hot" and "cold" patches, and the consequences for the synaptic strength will depend on the proximity of the input to the patches. Because in our model the potentiation prevailed, the same final effect can also be expected in patchy, thicker dendrites.

The mechanism of spatially nonuniform pattern formation is able, in itself, to produce noticeable long-term changes in the magnitude of the local EPSPs. However, the effects observed in the model could be further augmented by other Ca^{2+}-dependent processes in the postsynaptic cell, e.g., by Ca^{2+}-dependent change in the membrane conductances (Siegel et al., 1994) or phosphorylation of the membrane receptors (Jafee and Brown, 1994).

An important feature of our model is the presence of an NMDA-receptive metabotropic pathway participating in the activity-induced long-term changes in synaptic effectiveness. It is known that stimulation of metabotropic glutamate receptors can trigger the release of Ca^{2+} from intracellular stores through IP3 generation (Murphy and Miller, 1988; Llano et al., 1991; Berridge, 1993). Jafee and Brown (1994) have shown that activation of these receptors can produce localized increases in $[Ca^{2+}]_i$ that can propagate throughout the dendritic tree. Activation of metabotropic glutamate receptors can induce LTP without the participation of ionotropic receptors (Bortolotto and Collingridge, 1993). The metabotropic pathway was also thought to bridge the gap between the short-time and long-time electric behaviors of the neurons (Schiegg et al., 1995). Our results suggest a possible specific mechanism of NMDA metabotropic and ionotropic synergy in the modulation of synaptic efficacy.

We are grateful to Dr. S. Tyč-Dumont for support, encouragement, and valuable discussions.

This work was supported by the CNRS International Program for Scientific Cooperation (PICS 231 continuation).

REFERENCES

Asher, P., and L. Nowak. 1988a. Quisqualate and kainate-activated channels of mouse central neurons in culture. *J. Physiol. (Lond.).* 399: 227–245.

Asher, P., and L. Nowak. 1988b. The role of divalent cations in the *N*-methyl-D-aspartate responses of mouse central neurons in culture. *J. Physiol. (Lond.).* 399:247–266.

Bear, M. F., and R. C. Malenka. 1994. Synaptic plasticity: LTP and LTD. *Curr. Opin. Neurobiol.* 4:389–399.

Berridge, M. J. 1993. Inositol triphosphate and calcium signaling. *Nature.* 361:315–325.

Bezprozvanny, I., J. Watras, and B. E. Ehrlich. 1991. Bell-shaped calcium-response curves of $Ins(1,4,5)P_3$- and calcium-gated channels from endoplasmic reticulum of cerebellum. *Nature.* 351:751–754.

Bliss, T. V. P., and G. L. Collingridge. 1993. A synaptic model of memory: long-term potentiation in the hippocampus. *Nature.* 361:31–39.

Bootman, M. D., and M. J. Berridge. 1995. The elemental principles of calcium signaling. *Cell.* 83:675–678.

Bortolotto, Z. A., and G. L. Collingridge. 1993. A synaptic model of memory: long-term potentiation in the hippocampus. *Neuropharmacology.* 32:1–9.

Clapham, D. E., and J. Sneyd. 1995. Intracellular calcium waves. *Adv. Second Messenger Phosphoprotein Res.* 30:1–24.

Collingridge, G. L., and R. A. J. Lester. 1989. Excitatory amino acid receptors in the vertebrate central nervous system. *Pharmacol. Rev.* 40: 143–210.

Fewtrell, C. 1993. Ca^{2+} oscillations in non-excitable cells. *Annu. Rev. Physiol.* 55:427–454.

Friel, D. D. 1995. $[Ca^{2+}]_i$ oscillations in sympathetic neurons: an experimental test of a theoretical model. *Biophys. J.* 68:1752–1766.

Fromherz, P., and W. Zimmermann. 1995. Stable spatially periodic patterns of ion channels in biomembranes. *Phys. Rev. E.* 51:R1659–R1662.

Holmes, W. R., and W. B. Levy. 1990. Insights into associative long-term potentiation from computational model of NMDA receptor-mediated calcium influx and intracellular calcium concentration changes. *J. Neurophysiol.* 63:1148–1168.

Jafee, D. B., and T. H. Brown. 1994. Metabotropic glutamate receptor activation induces calcium waves within hippocampal dendrites. *J. Neurophysiol.* 72:471–474.

Kurata, K., K. Kisimoto, and E. Yanagida. 1989. The asymptotic transactional/circumferential homogeneity of the solutions of reaction-diffusion systems in/on cylinder-like domains. *J. Math. Biol.* 27: 485–490.

Llano, I., J. Dressen, M. Kano, and A. Konnerth. 1991. Intradendritic release of calcium induced by glutamate in cerebellar Purkinje cells. *Neuron.* 7:577–583.

Lynch, M. A., and T. V. Bliss. 1986. On the mechanism of enhanced release of [^{14}C]glutamate in hippocampal long-term potentiation. *Brain Res.* 369:405–408.

MacDermott, A. B., and N. Dale. 1987. Receptors, ion channels and synaptic potentials underlying the integrative actions of excitatory amino acids. *Trends Neurosci.* 10:280–284.

Malenka, R. C., and R. A. Nicoll. 1993. NMDA-receptor-dependent synaptic plasticity: multiple forms and mechanisms. *Trends Neurosci.* 16: 521–527.

Mayer, M. L., and G. L. Westbrook. 1987. The physiology of excitatory amino acids in the vertebrate central nervous system. *Prog. Neurobiol.* 28:197–276.

Murphy, S. N., and R. J. Miller. 1988. A glutamate receptor regulates Ca^{2+} mobilization in hippocampal neurons. *Proc. Natl. Acad. Sci. USA.* 85: 8737–8741.

Murray, J. D. 1989. Mathematical Biology. Springer-Verlag, Berlin (second corrected edition 1993).

Nicoll, R. A., and R. C. Malenka. 1995. Contrasting properties of two forms of long-term potentiation in the hippocampus. *Nature.* 377: 115–118.

Ross, C. A., J. Meldolesi, T. A. Milner, T. Satoh, S. Supattapone, and S. H. Snyder. 1989. Inositol 1,4,5,-triphosphate receptor localized to endoplasmic reticulum in cerebellar Purkinje neurons. *Nature.* 339:468–470.

Savtchenko, L. P., and S. M. Korogod. 1994. Domains of calcium channels as dissipative structures in a simulated neuron. *Neurophysiology.* 26: 99–107.

Schiegg, A., W. Gerstner, R. Ritz, and J. L. van Hemmen. 1995. Intracellular Ca^{2+} stores can account for the time course of LTP induction: a model of Ca^{2+} dynamics in dendritic spines. *J. Neurophysiol.* 74: 1046–1055.

Shepherd, G. M. 1972. The neuron doctrine: a revision of functional concept. *Yale J. Biol. Med.* 45:584–599.

Siegel, M., E. Marder, and L. F. Abbott. 1994. Activity-dependent current distributions in model neurons. *Proc. Natl. Acad. Sci. USA.* 91: 11308–11312.

Smith, G. D. 1985. Numerical Solutions of Partial Differential Equations: Finite Difference Methods. Oxford University Press, Oxford.

Smith, S. J. 1987. Progress on LTP at hippocampal synapses: a postsynaptic Ca^{2+} trigger for memory storage? *Trends Neurosci.* 10: 142–144.

Turing, A. M. 1952. The chemical basis of morphogenesis. *Philos. Trans. R. Soc. Lond. B.* 237:37–72.

Yamada, W. M., C. Koch, and P. R. Adams. 1989. Multiple channels and calcium dynamics. *In* Methods in Neuronal Modeling. From Synapses to Networks. C. Koch and I. Segev, editors. MIT Press, Cambridge, MA.